論文 / 著書情報
Article / Book Information

Title	Fabrication and characterization of rubidium/formamidinium-incorporated methylammonium-lead-halide perovskite solar cells
Authors	Masataka Kato, Atsushi Suzuki, Yuya Ohishi, Hiroki Tanaka, Takeo Oku
Citation	AIP Conference Proceedings, Vol. 1929, 1, pp. 020015-1-020015-7
Pub. date	2018, 1
Note	This article may be downloaded for personal use only. Any other use requires prior permission of the author and AIP Publishing. This article appeared in AIP Conference Proceedings, Vol. 1929, 1, pp. 020015-1-020015-7 and may be found at http://dx.doi.org/10.1063/1.5021928.

Fabrication and characterization of rubidium/formamidinium-incorporated methylammonium-lead-halide perovskite solar cells

Masataka Kato, Atsushi Suzuki, Yuya Ohishi, Hiroki Tanaka, and Takeo Oku

Citation: AIP Conference Proceedings **1929**, 020015 (2018); doi: 10.1063/1.5021928
View online: https://doi.org/10.1063/1.5021928
View Table of Contents: http://aip.scitation.org/toc/apc/1929/1
Published by the American Institute of Physics

Fabrication and characterization of rubidium/formamidinium-incorporated methylammonium-lead-halide perovskite solar cells

Masataka Kato, Atsushi Suzuki*, Yuya Ohishi, Hiroki Tanaka and Takeo Oku

Department of Materials Science, The University of Shiga Prefecture
2500 Hassaka, Hikone, Shiga, 522-8533, Japan

*Corresponding author: suzuki@mat.usp.ac.jp

Abstract. Fabrication and characterization of perovskite solar cells using mesoporous TiO_2 as an electron transporting layer and 2,2',7,7'-tetrakis-(*N,N*-di-4-methoxyphenylamino)-9,9'-spirobifluorene as a hole-transporting layer were performed for improving the photovoltaic performance. Additive effects of formamidinium (FA), rubidium (Rb), chlorine (Cl) and bromine (Br) into the methylammonium-lead-halide perovskite crystal on the photovoltaic properties and microstructures were investigated. The photovoltaic parameters of short-circuit current density, conversion efficiency, the surface morphology and domain in the perovskite crystal were characterized. The slight addition of FACl and RbBr to the $CH_3NH_3PbI_3$ crystal provided homogeneous microstructures with the dispersed crystal domains, which improved the photovoltaic performance. The excess addition of Cl to the perovskite crystal caused nanorod-like crystals, which degraded the photovoltaic performance.

INTRODUCTION

Fabrication and characterization of perovskite-based solar cells using mesoporous TiO_2 as an electron transporting layer and 2,2',7,7'-tetrakis-(*N,N*-di-4-methoxyphenylamino)-9,9'-spirobifluorene (Spiro-OMeTAD) as a hole-transporting layer (HTL) have been performed. There were many reports related on the photovoltaic properties and microstructures of methylammonium lead iodide ($CH_3NH_3PbI_3$: $MAPbI_3$) and formamidinium lead iodide ($HC(NH_2)_2PbI_3$: $FAPbI_3$) [1-4]. The mixed-cation lead halide perovskite solar cell using the $MAPbI_3$ and $FAPbI_3$ have advantages to control the bandgaps, which are related with carrier generation. The mixture of $MAPbX_3$ and $FAPbX_3$ varied with halogen in the metal-halogen ligand framework were used for application of the perovskite solar cell [5, 6]. Control of molar ratio between FA, MA, rubidium (Rb) as cations, iodine (I), bromine (Br), chlorine (Cl) as halogen atom in perovskite crystal will provide a best condition of the photovoltaic performance, the crystal structure, electronic structure and band gaps between highest occupied molecular orbital (HOMO) and lowest unoccupied molecular orbital (LUMO) and the optical absorption [7-10]. The insertion of both FA, MA, Rb, I, Br and Cl in the perovskite structure provided to promote carrier-generation and expanding carrier diffusion with reducing the charge trapping and recombination in the perovskite film for improvement of the photovoltaic performance [11-14].

The purpose of the present study is to investigate additive effect of FACl and RbBr to the $MAPbI_3$ perovskite crystal on the photovoltaic properties and microstructures. The photovoltaic properties, surface morphology and microstructures were investigated by current-voltage (*J-V*) curves under light irradiation, incident photon to current conversion efficiency, X-ray diffraction and optical microscopy. The photovoltaic properties depended on additive amount of FA, Br, Cl and Rb into the perovskite crystal.

EXPERIMENTAL

A schematic illustration for the fabrication of the present TiO_2/perovskite photovoltaic solar cells is shown in Fig. 1. F-doped tin oxide (FTO) substrates were cleaned using an ultrasonic bath with acetone and methanol, and dried under nitrogen gas. 0.15 And 0.30 M TiO_x precursor solution was prepared from titanium diisopropoxide

The Irago Conference 2017
AIP Conf. Proc. 1929, 020015-1–020015-7; https://doi.org/10.1063/1.5021928
Published by AIP Publishing. 978-0-7354-1621-5/$30.00

bis(acetylacetonate) (Sigma-Aldrich, 0.055 and 0.11 mL) with 1-butanol (1 mL), and the 0.15 M TiO_x precursor solution was spin-coated on the FTO substrate at 3000 rpm for 30 s and annealed at 125 °C for 5 min. Then, the 0.30 M TiO_x precursor solution was spin-coated on the TiO_x layer at 3000 rpm for 30 s and annealed at 125 °C for 5 min. This process of 0.30 M solution was performed two times, and the FTO substrate was sintered at 500 °C for 30 min to form the compact TiO_2 layer. After that, TiO_2 paste was coated on the substrate by spin-coating at 5000 rpm for 30 s. For the formation of mesoporous TiO_2 layer, the TiO_2 paste was prepared with TiO_2 powder with polyethylene glycol (PEG #20000) in ultrapure water. The solution was mixed with acetylacetone and triton X-100 for 30 min, and was left for 12 h to suppress the bubbles in the solution. The cells were annealed at 120 °C for 5 min and at 500 °C for 30 min to form the mesoporous TiO_2 layer. For the preparation of the perovskite compounds, a solution of CH_3NH_3I, PbI_2, $HC(NH_2)_2Br$, $HC(NH_2)_2Cl$ and RbBr with a desired mole ratio in γ-butyrolactone and DMF was mixed at 60 °C. The solution of perovskite compound was then introduced into the TiO_2 mesoporous by a spin-coating method and annealed at 125 °C for 15 min. Then, a hole-transport layer (HTL) was prepared by spin-coating. As the HTL, a solution of 2,2',7,7'-tetrakis[N,N-di(methoxyphenyl)amino]-9,9'-spirobifluorene (spiro-OMeTAD, 36.1 mg) in chlorobenzene was mixed with a solution of lithium bis(trifluoromethylsulfonyl)imide (Li-TFSI, 260 mg) in acetonitrile (0.5 mL) for 12 h. The former solution with 4-tert-butylpyridine (14.4 μL) was mixed with the Li-TFSI solution (8.8 μL) for 30 min at 70 °C. All procedures were carried out in ordinary air. Finally, gold (Au) metal contacts were evaporated as top electrodes. Layered structures of the present photovoltaic cells were denoted as FTO/TiO_2/perovskite/spiro-OMeTAD/Au, as shown in a schematic illustration of Fig. 1. The J–V characteristics of the photovoltaic cells were measured under illumination at 100 mW cm^{-2} by using an AM 1.5 solar simulator. The solar cells were illuminated through the side of the FTO substrates, and the illuminated area was 0.090 cm^2. The IPCE of the cells were also investigated. The microstructures of the thin films were observed by using an optical microscope.

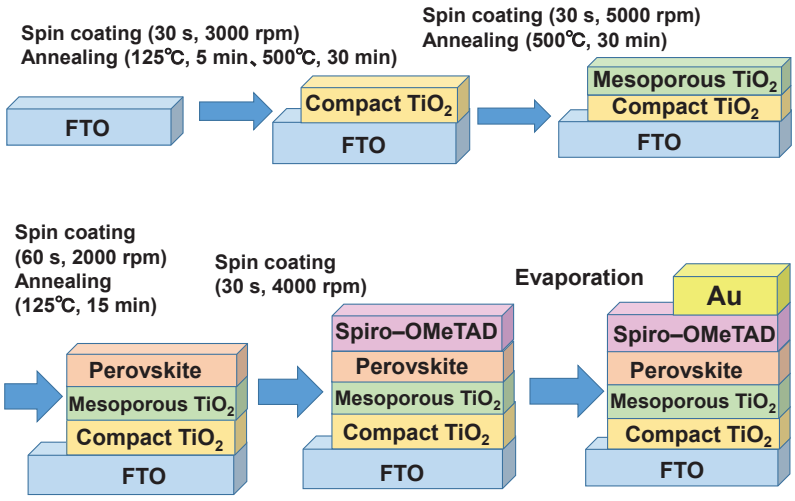

FIGURE 1. Schematic illustration for the fabrication of the present perovskite solar cells.

RESULTS AND DISCUSSION

Figure 2 is *J–V* characteristics of the TiO_2/perovskite/spiro-OMeTAD photovoltaic devices under illumination. The photocurrent under illumination of the perovskite solar cells showed semi-conductive characteristic curves with regard to the short-circuit current density (J_{sc}) and open-circuit voltage (V_{oc}). The measured photovoltaic parameters of the $CH_3NH_3PbI_3$ devices are summarized as listed in Table 1. In the case of the $MAPbI_3$ cell, the photovoltaic parameters of V_{OC}, the short-circuit current density, J_{SC}, overall power conversion efficiency (η), series resistance (R_S), and the shunt resistance (R_{sh}) were obtained to be 0.897 V, 12.83 mA cm^{-2}, 6.70 %, 11 Ω cm^{-2}, 595 Ω cm^{-2} as listed in Table 1. When 5% FACl and RbBr was added into the $MAPbI_3$ crystal phase, the $MA_{0.90}FA_{0.05}Rb_{0.05}PbI_{2.90}Br_{0.05}Cl_{0.05}$ perovskite compound generated as reaction product. The perovskite solar cell characterized with providing improvement of the photovoltaic parameters for the η of 7.70 %, a fill factor (*FF*) of 0. 670, J_{SC} of 13.22 mA cm^{-2}, V_{OC} of 0.873 V, R_S of 6 Ω cm^{-2}, and R_{sh} of 736 Ω cm^{-2}, respectively. The slight addition of Cl as halogen into the

perovskite crystal improved the photovoltaic performance of J_{sc}, FF and η, due to improvement of carrier generation, carrier diffusion and charge separation. The decrease of the photovoltaic parameter of R_S was based on improvement of the integral conductivity related to its internal carrier mobility in the perovskite crystal. The behavior of R_{sh} referred the loss of photocurrent caused to carrier recombination within the device, particularly at the interfaces of each layer in the perovskite solar cell. EQE of the perovskite solar cells varied with percentage of Br or Cl as halogen are shown in Fig. 3. In the absence of FA and Br, the EQE of the solar cell was covered in the range of 320 nm-800 nm. When FA, Br, Cl and Rb were largely added into the $FAPbI_2Br$ crystal, the intensity of EQE was decreased. These behavior were based on suppression of carrier generation and diffusion with trapping and recombination near the domain in the crystal. The perovskite solar cells had the photovoltaic performance in the range of 310 nm-790 nm, which almost agreed with the reported energy band gap for $CH_3NH_3PbI_3$ perovskite crystal.

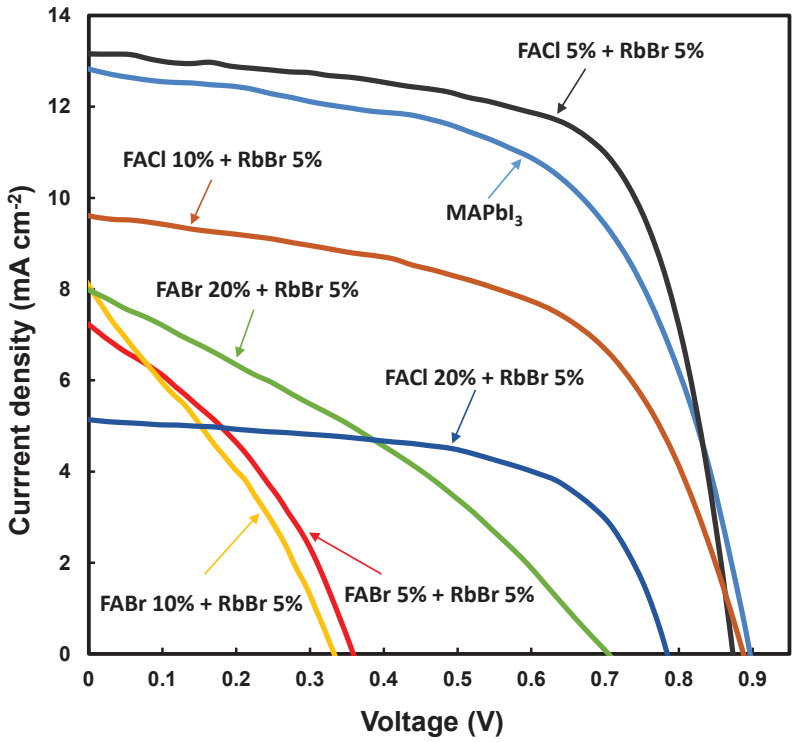

FIGURE 2. Light-induced *J-V* curves of the perovskite solar cells doped with FACl, FABr and RbBr.

TABLE 1. Photovoltaic parameters of the present perovskite solar cells.

Sample	J_{SC} (mA cm^{-2})	V_{OC} (V)	*FF*	η (%)	R_s (Ω cm^{-2})	R_{sh} (Ω cm^{-2})
$MAPbI_3$	12.83	0.897	0.583	6.70	11	595
FABr 5% + RbBr 5%	7.21	0.359	0.362	0.94	114	965
FABr 10% + RbBr 5%	8.08	0.333	0.301	0.81	27	56
FABr 20% + RbBr 5%	7.98	0.705	0.325	1.83	32	128
FACl 5% + RbBr 5%	13.22	0.873	0.670	7.70	7	736
FACl 10% + RbBr 5%	9.61	0.887	0.559	4.77	17	487
FACl 20% + RbBr 5%	5.14	0.784	0.601	2.42	13	1070

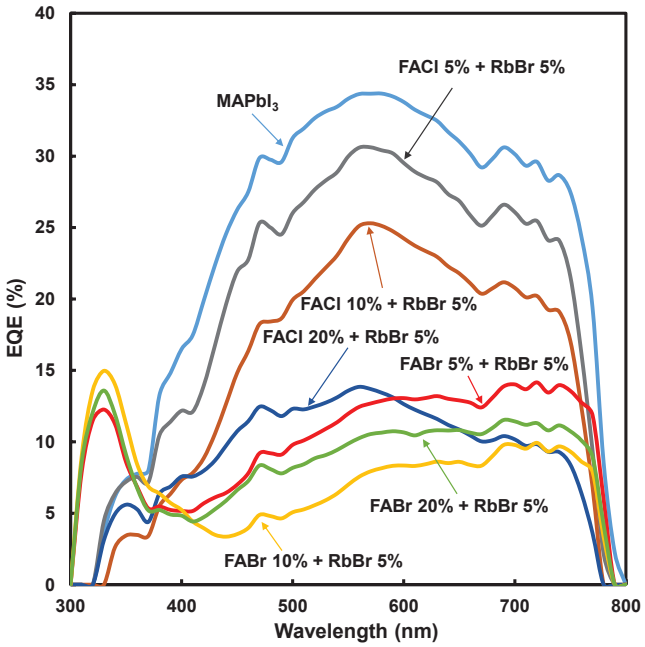

FIGURE 3. EQE of the present perovskite solar cells doped with FACl, FABr and RbBr.

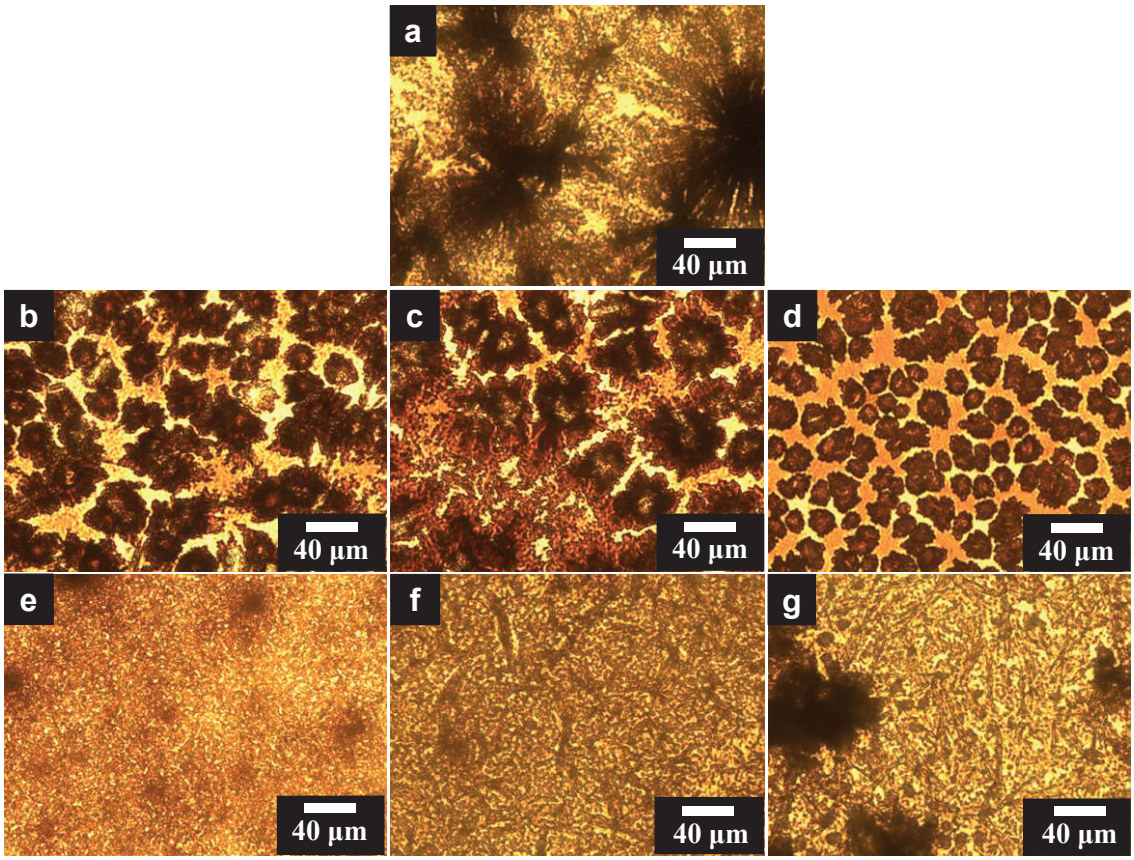

FIGURE 4. Surface morphology of the perovskite solar cells using (a) $MAPbI_3$ doped with (b) FABr 5%, RbBr 5%, (c) FABr 10%, RbBr 5%, (d) FABr 20%, RbBr 5%, (e) FACl 5%, RbBr 5%, (f) FACl 10%, RbBr 5%, (g) FACl 20% and RbBr 5%.

Surface morphology of the perovskite solar cells are shown in Fig. 4 (a)-(g). In the case of the $CH_3NH_3PbI_3$ solar cell as shown in Fig. 4 (a), the needle-like crystals with black domains at the size of 120 μm were dispersed on the mesoporous TiO_2 layer. In the case of the $MA_{1-X}FA_XRb_{0.05}PbI_{2.95-X}Br_{0.05+X}$ perovskite solar cells as shown in Fig. 4 (b)-(d), the slight addition of Br caused the dispersion of the perovskite aggregation with crystal domain in the range of 40-60 μm. The excessive amount of Br provided the heterogeneous phase with the separated domain. In the case of the $MA_{1-X}FA_XRb_{0.05}PbI_{2.95-X}Br_{0.05}Cl_X$ cell as shown in Fig. 4(e)-(g), the homogenous microstructure with the fine structure based on the dispersed domain at size of 10 μm was observed. The slight addition of FACl and RbBr at 5% caused appearance of the dispersed domain in the microstructure. The excessive addition of Cl into the perovskite crystal caused to produce the crystal nucleation and growth of long one-dimensional nanorod-like crystal as the hexagonal non-perovskite phase. The addition of FACl and RbBr into the perovskite crystal influenced the crystal growth mechanism in the heterogeneous microstructure, which suppressed the photovoltaic performance with trapping and recombination of carrier near the domain.

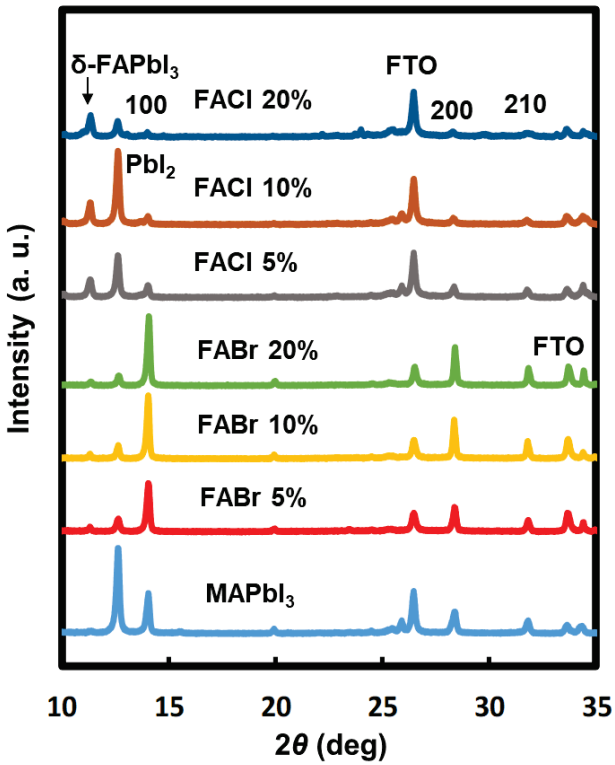

FIGURE 5. X-ray diffraction patterns of the perovskite solar cells doped with FACl, FABr and RbBr.

TABLE 2. X-ray diffraction parameters of 100 of the perovskite solar cells doped with FACl, FABr and RbBr.

Sample	2θ (°)	d (Å)
$MAPbI_3$	14.06	6.292
FABr 5% + RbBr 5%	14.07	6.289
FABr 10% + RbBr 5%	14.05	6.297
FABr 20% + RbBr 5%	14.09	6.280
FACl 5% + RbBr 5%	14.05	6.299
FACl 10% + RbBr 5%	14.03	6.307
FACl 20% + RbBr 5%	14.01	6.315

X-ray diffraction patterns of the perovskite solar cells added with FACl and FABr are shown in Fig. 5. The diffraction patterns of $MAPbI_3$ perovskite crystal were identified as remarks. A strong diffraction peak in 2θ was obtained to be 14.06 °, corresponding to be about 6.292 Å in d-spacing. The spacing at 14.06 ° was assigned to be (100) surface of the perovskite crystal. Table 2 lists the diffraction parameters of 100 of the perovskite crystal added by FABr, FACl and RbBr. The peak around 12.7 ° was considered to be the peak of PbI_2. The intensity of the peak was decreased with increasing the percentage of FABr. The crystal growth with increase of crystalline domain size was obtained with increasing the amount of FABr at 20%. When FACl was added from 5% to 20%, the peak was shifted in the low angle side. The lattice constant was increased with increasing the percentage of FACl. The peaks around 11.4 ° are considered to be the peaks of the hexagonal non-perovskite phase (δ- $FAPbI_3$) [15,16]. The phase formation of $FAPbI_3$ with different polymorphs in the process condition was important factor for optimizing with tuning the photovoltaic performance based on charge transport near the domain in the perovskite crystal.

The halogen of Br and Cl ions into the perovskite crystal influenced the crystal nucleation and growth, and the crystal lattice constant in the heterogeneous microstructure, which affected to the electronic structure, band gap, the carrier diffusion, charge transport, and the photovoltaic performance of J_{sc}, V_{oc} and η. The role of Cl as halogen on the charge transport and the photovoltaic properties has been discussed. Incorporation of Cl into the perovskite crystal remarkably affected the surface morphology, crystal nucleation and growth and the photovoltaic performance of J_{sc} and η. Control of weight percentage of FACl and RbBr is important factor to optimize with tuning the condition of the carrier generation and charge transport for improvement of the photovoltaic performance of J_{sc} and η.

The photovoltaic mechanism of the perovskite solar cells added with FA, Cl, Br and Rb is discussed on the basis of energy level. Light irradiation induced the generating and charge separation in the perovskite crystal as the active layer. The excited electrons of the perovskite crystal in the conduction band slightly diffused and charges transferred from the perovskite crystal to TiO_2 on the active layer at an FTO substrate, and holes in valence band went through spirobifluorence as hole-transporting layer and arrived at the Au electrode as the cathode. An energy barrier would exist at the semiconductor–metal interface. The V_{oc} of the perovskite solar cells would be related to the energy gap between the valence band of the perovskite crystal and conduction band of TiO_2. The energy levels of the highest occupied molecular orbital, band gap and the carrier mobility of hole-transport layer can be controlled by addition of hydrogens and Rb. The slight incorporation of Cl and Rb into the perovskite crystal influenced the surface morphology in the homogenous microstructure with the dispersed domain, which improved the photovoltaic performance of J_{sc}, FF and η. The carrier diffusion and charge transport in the perovskite single crystals would be improved by the addition of FACl and RbBr. The carrier mobility of the perovskite layer was depending on the condition of the surface morphology with the dispersed crystal domain, and extent of unreacted perovskite compound in the perovskite layer. With excess amount of halogen into the perovskite crystal, the photovoltaic performance might be fluctuated and reduced by suppression of carrier generation and diffusion with trapping and recombination of the carriers near the domain in heterogeneous microstructure. Additive control of hydrogen and Rb in the perovskite crystal is important factor to optimize with tuning the condition of the carrier generation, charge transport with suppression of trapping and recombination of carrier near the domain in the perovskite crystal.

CONCLUSION

The perovskite-based photovoltaic devices varied with amount of halogen and Rb were fabricated and characterized. The additive effects of FACl and RbBr into the $MAPbI_3$ perovskite crystal on the photovoltaic properties, surface morphology and microstructure were investigated. The surface morphology showed a different behavior of crystal growth and microstructure depending on extent of Br and Cl. The addition of Cl and Br into the perovskite crystal changed from the homogeneous microstructure with the dispersed domain to the heterogeneous phase. The X-ray diffraction identified concentration dependence of Cl and Rb on the crystal growth. The slight addition of Cl and Rb into the perovskite crystal provided the homogenous phase with the small size domain, which improved the photovoltaic performance of J_{sc}, FF and η. The excessive addition of Cl into the perovskite crystal caused to produce the crystal growth of long one-dimensional nanorod-like crystal in the heterogeneous phase, which suppressed the photovoltaic performance. Additive control of amount of hydrogen and Rb in the perovskite crystal is important factor to optimize with tuning the carrier generation, charge transport with suppression of trapping and recombination of carrier near the domain. Energy diagram and photovoltaic mechanism of the perovskite solar cells varied with halogen and Rb was discussed.

ACKNOWLEDGMENT

This work was partly supported by Satellite Cluster Program of the Japan Science and Technology Agency.

REFERENCES

1. G. E. Eperon, S. D. Stranks, C. Menelaou, M. B. Johnston, L. M. Herz and H. J. Snaith, Energy. Environ. Sci **7**, 982-988 (2014).
2. S. Aharon, A. Dymshits, A. Rotem and L. Etgar, Journal. Mat. Chem A **3**, 9171-9178 (2015).
3. C. Yi, J. Luo, S. Meloni, A. Boziki, N. A. Astani, C. Grätzel, S. M. Zakeeruddin, U. Röthlisberger and M. Grätzel, Energy. Environ. Sci **9**, 656-662 (2016).
4. G. Li, T. Zhang, F. Xu and Y. Zhao, Mater. Today Energy. **5**, 293-298 (2017).
5. D. P. McMeekin, G. Sadoughi, W. Rehman, G. E. Eperon, M. Saliba, M. T. Hörantner, A. Haghighirad, N. Sakai, L. Korte, B. Rech, M. B. Johnston, L. M. Herz and H. J. Snaith, Science **351**, 151-155 (2016).
6. J. Kim, N. Parkb, J. S. Yun, S. Huang, M. A. Green and A. W. Y. H. Baillie, Sol. Energy Mater. Sol. Cells. **162**, 41-46 (2017).
7. M. Hu, L. Liu, A. Mei, Y. Yang, T. Liu and H. Han, Journal. Mat. Chem. A **2**, 17115-17121 (2014).
8. D. Prochowicz, P. Yadav, M. Saliba, M. Saski, S. M. Zakeeruddin, J. Lewiński and M. Grätzel, Sustainable Energy & Fuels **1**, 689-693 (2017).
9. N. J. Jeon, J. H. Noh, W. S. Yang, Y. C. Kim, S. Ryu, J. Seo and S. Il Seok, Nature **517**, 476-480 (2015).
10. M. Saliba, T. Matsui, K. Domanski, J. Y. Seo, A. Ummadisingu, S. M. Zakeeruddin, J. P. C. Baena, W. R. Tress, A. Abate, A. Hagfeldt and M. Grätzel, Science **354**, 206-209 (2016).
11. P. Yadav, M. I. Dar, N. Arora, E. A. Alharbi, F. Giordano, S. M. Zakeeruddin, M. Grätzel, Adv. Mater. **29**, 1701077-1701085 (2017).
12. B. Philippe, M. Saliba, J. P. C. Baena, U. B. Cappel, S. H. T. Cruz, M. Grätzel, A. Hagfeldt, and H. Rensmo, Chem. Mater. **29**, 3589-3596 (2017).
13. J. You, Z. Hong, Y. M. Yang, O. Chen, M. Cai, T. Song, C. Chen, S. Lu, Y. Liu, H. Zhou and Y. Yang, ACS Nano **8**, 1674-1680 (2014).
14. Y. H. Park, I. Jeong, S. Bae, H. J. Son, P. Lee, J. Lee, C. H. Lee and M. J. Ko, Adv. Fun. Mater. **27**, 1605988-1605997 (2017).
15. S. Prathapani, D. Choudhary, S. Mallick, P. Bhargava and A. Yella, CrystEngComm, 19, 3834-3843 (2017).
16. V. L. Pool, B. Dou, D. G. V. Campen, T. R. K. Stockert, F. S. Barnes, S. E. Shaheen, M. I. Ahmad, M. F. A. M. Hest and M. F. Toney, Nat. Commun. **8**, 14075-14083 (2017).